Noninvasive *in vivo* imaging of oxygen metabolic rate in the retina*

Wenzhong Liu and Hao F. Zhang

***Abstract*— Precise and noninvasive measurement of retinal oxygen metabolic rate is important for retinal pathological investigations as well as retinal disease detection, which has not been achieved until recently. Here, we quantified retinal oxygen metabolic rate in rats by combining photoacoustic ophthalmoscopy with spectral domain-optical coherence tomography. We employed multi-wavelength photoacoustic ophthalmoscopy for oxygen saturation measurement and applied dual-ring scanning Doppler spectral domain-optical coherence tomography to image retinal blood flow. With retinal oxygen saturation and blood flow being measured, we determined the retinal oxygen metabolic rate in a typical rat to be 373.41 ± 88.04 ng/minute.**

I. Introduction

Blindness and low vision have affected more than 3 million Americans aged 40 years and older by 2004; more than 80% of such visual impairments were caused by diseases originating in the eye [1]. Major causes of visual impairments include glaucoma, diabetic retinopathy (DR), age-related macular degeneration (AMD), cataracts and so on. Complications of oxygen metabolism are reported to be involved in most of these diseases [2, 3]. For example, hypoxia can damage the optic nerve head, partially due to insufficient vascular perfusion in the glaucomatous retina [4]; in DR, variation of retinal blood flow is caused by pericyte loss, which further leads to retinal vascular occlusion and retinal hypoxia [5]. Thus, precise measurement of retinal oxygen metabolic rate (rMRO2) can be critical in investigating these blinding diseases.

Despite the importance of rMRO2, accurate and noninvasive measurement has not yet been achieved; the difficulty lies in the challenge that rMRO2 measurement requires detection of retinal blood flow and oxygen saturation (sO_2) together, and preferably simultaneously. To date, advancements in Doppler spectral domain-optical coherence tomography (SD-OCT) facilitates accurate detection of blood flow [6]; the main obstacle for rMRO2 comes from retinal sO_2 measurement. To achieve retinal sO_2 noninvasively, researchers have employed multi-spectral fundus photography, yet the sO_2 measurement accuracy and repeatability is poor, with measurement error up to 20% confirmed by numerical simulation studies [7]. We recently applied visible-light optical coherence tomography (Vis-OCT) to quantify retinal sO_2 *in vivo* [8], but significant challenges still exist before Vis-OCT can be verified at various anatomical sites for accurate sO_2 measurement.

Photoacoustic (PA) imaging can sense sO_2 quantification accurately in a noninvasive manner by the merit of direct measurement of light absorption within blood [9]; experimentally, promising sO_2 results have already been reported in many tissues and organs such as the ear [10], brain [11] and so on. Building on the established capabilities of PA imaging, we developed photoacoustic ophthalmoscopy (PAOM) [12, 13], which can assess light absorption properties of retinal vessels by detecting laser-induced ultrasonic signals from hemoglobin, guaranteeing accurate retinal sO_2 measurement. We employed multi-wavelength PAOM to uncover retinal sO_2, and, subsequently, the rMRO2 by integrating PAOM with Doppler SD-OCT.

II. Methods and Materials

A. Imaging System

The details regarding our imaging modality can be found in our previous paper [12]. Briefly, as shown in Figure 1,

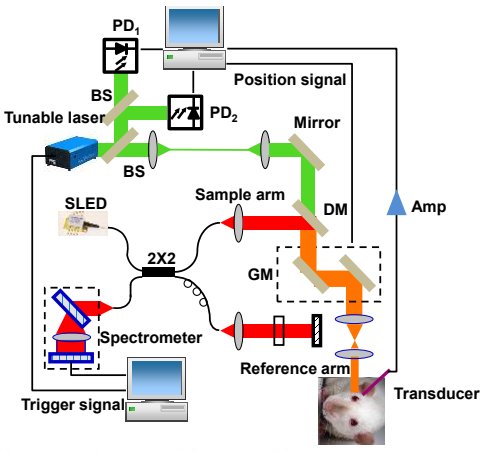

Figure 1. Diagram of the optical imaging system. SLED: super luminescent diode; BS: beam splitter; GM: galvanometer; DM: dichroic mirror; Amp: amplifier; PD: photodetector.

probing light from SD-OCT and PAOM were combined, aligned and focused onto the rat retina. In SD-OCT, backscattered photons from the retina interfere with reference photons and were collected by a home-made spectrometer. In PAOM, laser-induced ultrasonic waves were first acquired by an ultrasonic transducer (40-MHz central frequency, 15-MHz bandwidth at 70% amplitude, 0.5×0.5 mm^2 active element size), then amplified and digitized. In our experiment, the A-line rate was set at 25 kHz. To acquire a fundus image, we raster scanned the optical illumination to obtain 256×256 A-lines in both SD-OCT and PAOM. For blood sO_2 and flow imaging, we employed a circular scanning method; each

*Resrach supported by the NIH grants 1R01EY019951 and 1R24EY022883. NSF grant CBET-1055379.

Wenzhong Liu is with the Biomedical Engineering Department, Northwestern University, Evanston, Illinois, 60208, USA. Wenzhong Liu is an HHMI international student research fellow (e-mail: wenzhongliu2016@u.northwestern.edu).

Hao F. Zhang is with the Biomedical Engineering Department, Northwestern University Evanston, Illinois, 60208, USA, as well as the Ophthalmology Department, Northwestern University, Chicago, IL 60611, USA (phone: 847-491-2946; fax: 847-491-4928; e-mail: hfzhang@northwestern.edu)

circular B-scan contained 4096 A-lines; we performed eight consecutive retinal scans of small and big rings centered at the optic disc. The lateral resolutions of both PAOM and OCT are about 20μm; the axial resolutions of PAOM and OCT are 23 and 7 μm, respectively. To ensure ocular laser safety, the PAOM laser pulse energy was set lower than 40 nJ.

B. Animal Preparation

The animal preparation procedure was as described in our previous paper [12]. Briefly, we imaged albino rats (Sprague Dawley, 500 g, Harlan Laboratories, Indianapolis, IN). In experiments, the animals were first anesthetized by a mixture of 1.5% isoflurane and regular air; then we dilated the rats' pupils with 1% tropicamide ophthalmic solution and paralyzed the iris sphincter muscle with 0.5% tetracaine hydrochloride ophthalmic solution. Meanwhile, artificial tear drops (Systane, Alcon Laboratories, Inc.) were applied every minute to prevent corneal dehydration. All animal experimental procedures were approved by the Institutional Animal Care and Use Committee at Northwestern University.

C. sO2 Quantification

Details of retinal sO_2 calculation can be found in [7]. In PAOM, we used three wavelengths: 570, 578, 588 nm for retinal sO_2 measurement. The optical absorption coefficient of blood can be expressed by:

$$\mu_a(\lambda_i) = \ln(10) \times (\varepsilon_{HbO_2}(\lambda_i) \times [HbO_2] + \varepsilon_{HbR}(\lambda_i) \times [HbR]), \quad (1)$$

where *[HbR]* and *[HbO_2]* are concentrations of the deoxygenated and oxygenated hemoglobin, respectively; $\mathcal{E}_{\mathrm{HbR}}(\lambda_i)$ and $\mathcal{E}_{\mathrm{HbO2}}(\lambda_i)$ are the known molar extinction coefficients [$cm^{-1}M^{-1}$] of *HbR* and *HbO_2* at wavelength λ_i [nm]. Since energy deposition $\phi(\lambda_i,x,y,z)$ is proportional to the local optical absorption coefficient; given no detection saturation, we can use $\phi(\lambda_i,x,y,z)$ instead of $\mu_a(\lambda_i)$ for estimating the relative *[HbR]* and *[HbO_2]* values. As a result, we have:

$$\begin{bmatrix} [HbR] \\ [HbO_2] \end{bmatrix} = (M^T M)^{-1} M^T \Phi(x,y,z) K, \quad (2)$$

where

$$M = \begin{bmatrix} \varepsilon_{HbR}(\lambda_1) & \varepsilon_{HbO_2}(\lambda_1) \\ \vdots & \vdots \\ \varepsilon_{HbR}(\lambda_n) & \varepsilon_{HbO_2}(\lambda_n) \end{bmatrix}, \qquad \Phi(x,y,z) = \begin{bmatrix} \phi(\lambda_1,x,y,z) \\ \vdots \\ \phi(\lambda_n,x,y,z) \end{bmatrix}$$

and K is an unknown proportionality coefficient. Although K is unknown, the calculated sO_2 is absolute, which can be determined by (3).

$$sO_2(x,y,z) = \frac{[HbO_2]_{(x,y,z)}}{[HbO_2]_{(x,y,z)} + [HbR]_{(x,y,z)}}, \quad (3)$$

D. Blood Flow Quantification

Blood velocity and vessel size are two necessities for blood flow quantification. The flow velocity v [m/s] in SD-OCT is determined by [6]:

$$v = \frac{f_{sample} \times \lambda_0 \times \Delta\phi}{4 \times \pi \times n \times \cos(\theta)}, \quad (4)$$

where f_{sample} [kHz] is the OCT axial scan frequency, λ_0 [nm] is the center wavelength of the light source, $\Delta\phi$ is the Doppler effect induced phase shift [degree], n is the refractive index of the sample, and θ [radians] is the Doppler angle, which is the angle between blood flow and probing light. To achieve phase shift and Doppler angle simultaneously, Dual-ring scanning in SD-OCT was employed [6, 14], where details about Doppler angle calculation can be found in [6].

We measured the vessel diameter axially in the OCT B-scan amplitude image because of the high axial resolution capailities of OCT. If we denote the vessel diameter in the B-scan as *Dia* [m], the actual vessel diameter *Dia_r* [m] is:

$$Dia\_r = Dia \times \sin(\theta), \quad (5)$$

where θ [radians] is the Doppler angle. The vessel cross-sectional area A [m^2] is calculated by:

$$A = \pi \times \frac{Dia\_r^2}{4}, \quad (6)$$

Then the blood flow is:

$$F_i = v_i \times A_i, \quad (7)$$

where i denotes the i_{th} vessel.

E. rMRO2 quantification

With retinal sO_2 and blood flow, the rMRO2 [g/minute] is calculated as:

$$rMRO2 = \frac{60 \times 4 \times W_{O2}}{W_{HbO2}} \times [HbT] \times (sO_{2a} \times F_a - sO_{2v} \times F_v), \quad (8)$$

where W_{O2} and W_{HbO2} are the molecular weights of O_2 and oxyhemoglobin, which are 32 and 68000 [g/mol], respectively; *[HbT]* is the total concentration of hemoglobin in the rat, which is measured to be 150 [g/L] in current studies; $sO_{2\alpha}$ and sO_{2v} are oxygen saturation values in the arterial and venous systems, respectively; F_α and F_v are the total flow in arterial and venous retinal vascular systems.

III. Results

A. Retinal sO_2

The retinal fundus image from PAOM can be obtained through a maximum-amplitude-projection of the acquired volumetric data; a sample fundus image of an albino rat retina is shown in Figure 2a with major retinal vessels being labeled from 1 to 12. The white ring indicates where multi-wavelength scans were performed for sO_2 interrogation. Figure 2b shows one sample circular B-scan PAOM image at 570 nm, collected from the position highlighted by the white ring in Figure 2a. The light absorption by retinal blood can then be obtained. Figure 2c gives light absorption coefficients of oxyhemoglobin (*HbO2*) and deoxyhemoglobin (*HbR*). Statistics results of retinal sO_2 values from circular B-scan images are given in Figure 2d, where it shows that the mean sO_2 value for arterioles is 93.0±3.5 %, and for venules is 77.3±9.1%, which are within the normal range [15].

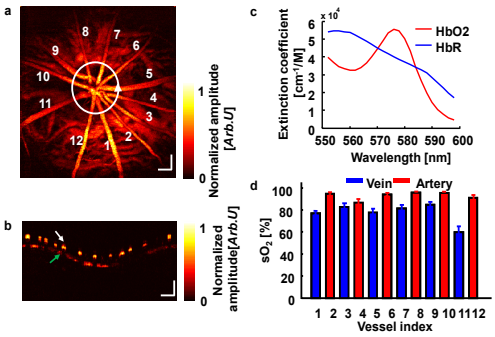

Figure 2. Retinal sO_2 results measured by PAOM. (a) Retinal fundus image acquired by PAOM. (b) Sample B-scan image along the white ring in (a), the white arrow indicates retinal vasculature, green arrow shows choroidal vessels. (c) Extinction coefficient spectrum of oxy-hemoglobin and de-oxy hemoglobin. (d) Statistic results of retinal sO_2. Bar: 200 µm.

B. Retinal Blood Flow

The blood flow results are shown in Figure 3.

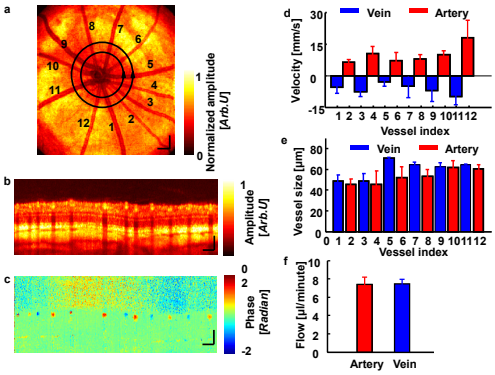

Figure 3. Retinal flow results measured by Doppler SD-OCT. (a) Retinal fundus image acquired by OCT, two-black rings show where the dual-ring scanning were performed. (b) OCT amplitude B-scan image from the inner ring scan indicated in (a). (c) OCT phase B-scan image from the inner ring scan indicated in (a). (d) Statistic results of flow velocity in each vessel. (e) Statistic results of vessel size for each vessel. (f) Statistic results of total flow in retinal arteries and veins. Bar: 200 µm.

An OCT fundus retinal image is given in Figure 3a, with twelve vessels being labeled. Dual-ring scanning positions on the retina are indicted by two black rings centered at the optic disc, with radii of 0.45 and 0.56 mm. One sample B-scan amplitude SD-OCT image and raw phase SD-OCT image from the inner circular scan is given in Figure 3b and c. Statistical results of velocities from the twelve vessels are given in Figure 3d, from which we can tell the velocities in arteries are higher than velocities in corresponding veins. Vessel diameters are given in Figure 3e, from which we also can tell that veins have an average larger vessel size than corresponding arteries. By multiplying blood velocity with vessel cross-sectional size, we can achieve total retinal blood flow, which is 7.43 ± 0.51 µl/minute for the venous vascular system; and 7.38 ±0.78 µl/minute for the arterial vascular system (Figure 3f). Our results are consistent with previously reported results [16]. With the sO_2 and flow being measured, we determined rMRO2 to be 373.41 ± 88.04 ng/minute.

IV. Conclusion and Discussion

In the present study, for the first time, we successfully demonstrated that *in vivo* rMRO2 can be quantified noninvasively and precisely by integrating PAOM and Doppler SD-OCT. The proposed imaging modality can be a powerful tool for the investigation of the pathophysiology of retinal diseases and retinal disease detection in clinical practice. Despite the advantages, our imaging modality still has limitations. One of the concerns is that ultrasonic signal detection requires physical contact between transducer and tissue sample [12], which is inconvenient. Developments in non-contact ultrasonic signal detection can make our imaging modality more feasible for clinic trials. Another concern is that blood flow measurement may be influenced by eye movement due to the consecutive and non-simultaneous scanning sequence of the small and big ring in dual-ring scanning SD-OCT. In the present study, we average the results across eight pairs of small-big rings to reduce the influence of eye movement. One more promising alternative to reduce the influence of eye motion may involve scanning the small and big rings simultaneously as demonstrated in our recent study [17].

Acknowledgment

We would like to thank Dr. Yi Ji, Prof. Nader Sheibani, Prof. Robert A. Linsenmeier and Prof. Amani A. Fawzi for helpful discussion. We also thank Kevin Zhang for proofreading the manuscript.

References

[1] N. Congdon, B. O'colmain, C. Klaver, R. Klein, B. Munoz, D. Friedman, et al., "Causes and prevalence of visual impairment among adults in the United States," *Arch. Ophthalmol.*, vol. 122, pp. 477-485, Apr 2004.

[2] D. Y. Yu and S. J. Cringle, "Oxygen distribution and consumption within the retina in vascularised and avascular retinas and in animal models of retinal disease," *Prog. Retin. Eye Res.*, vol. 20, pp. 175-208, Mar 2001.

[3] D. Y. Yu and S. J. Cringle, "Retinal degeneration and local oxygen metabolism," *Exp. Eye Res.*, vol. 80, pp. 745-51, Jun 2005.
[4] G. Tezel and M. B. Wax, "Hypoxia-inducible factor 1 {alpha} in the glaucomatous retina and optic nerve head," *Arch. Ophthalmol.*, vol. 122, pp. 1348-1356, Sep 2004.
[5] E. M. Kohner, V. Patel, and S. Rassam, "Role of blood flow and impaired autoregulation in the pathogenesis of diabetic retinopathy," *Diabetes*, vol. 44, pp. 603-607, Jun 1995.
[6] Y. Wang, B. A. Bower, J. A. Izatt, O. Tan, and D. Huang, "Retinal blood flow measurement by circumpapillary Fourier domain Doppler optical coherence tomography," *J. Biomed. Opt.*, vol. 13,pp. 064003, Nov 2008.
[7] W. Liu, S. Jiao, and H. F. Zhang, "Accuracy of retinal oximetry: a Monte Carlo investigation," *J. Biomed. Opt.*, vol. 18, pp. 066003, Jun 2013.
[8] J. Yi, Q. Wei, W. Liu, V. Backman, and H. F. Zhang, "Visible-light optical coherence tomography for retinal oximetry," *Opt. Lett.*, vol. 38, pp. 1796-8, Jun 1 2013.
[9] H. F. Zhang, K. Maslov, M. Sivaramakrishnan, G. Stoica, and L. V. Wang, "Imaging of hemoglobin oxygen saturation variations in single vessels in vivo using photoacoustic microscopy," *Appl. Phys. Lett.*, vol. 90, pp. 053901, 2007.
[10] J. Yao, K. I. Maslov, Y. Zhang, Y. Xia, and L. V. Wang, "Label-free oxygen-metabolic photoacoustic microscopy in vivo," *J. Biomed. Opt.*, vol. 16, pp. 076003, Jul 2011.
[11] S. Hu, K. Maslov, V. Tsytsarev, and L. V. Wang, "Functional transcranial brain imaging by optical-resolution photoacoustic microscopy," *J. Biomed. Opt.*, vol. 14, pp. 040503, Jul 2009.
[12] W. Song, Q. Wei, T. Liu, D. Kuai, J. M. Burke, S. Jiao, et al., "Integrating photoacoustic ophthalmoscopy with scanning laser ophthalmoscopy, optical coherence tomography, and fluorescein angiography for a multimodal retinal imaging platform," *J. Biomed. Opt.*, vol. 17, pp. 061206, Jun 2012.
[13] W. Song, Q. Wei, L. Feng, V. Sarthy, S. Jiao, X. Liu, et al., "Multimodal photoacoustic ophthalmoscopy in mouse," *J. Biophotonics*, vol.6, pp.505-512, Jun 2013.
[14] H. Wehbe, M. Ruggeri, S. Jiao, G. Gregori, C. A. Puliafito, and W. Zhao, "Automatic retinal blood flow calculation using spectral domain optical coherence tomography," *Opt. Express*, vol. 15, pp. 15193-15206, Nov 2007.
[15] D. F. Wilson, S. A. Vinogradov, P. Grosul, M. N. Vaccarezza, A. Kuroki, and J. Bennett, "Oxygen distribution and vascular injury in the mouse eye measured by phosphorescence-lifetime imaging," *Appl. Opt.*, vol. 44, pp. 5239-48, Sep 1 2005.
[16] W. Choi, B. Baumann, J. J. Liu, A. C. Clermont, E. P. Feener, J. S. Duker, et al., "Measurement of pulsatile total blood flow in the human and rat retina with ultrahigh speed spectral/Fourier domain OCT," *Biomed. Opt. Express*, vol. 3, pp. 1047-61, May 1 2012.
[17] C. Dai, X. Liu, H. F. Zhang, C. A. Puliafito, and S. Jiao, "Absolute retinal blood flow measurement with a dual-beam Doppler optical coherence tomography," *Invest. Ophthalmol. Vis. Sci.,* vol. 54, pp. 7998-8003, Dec 2013.